Journal of Organometallic Chemistry 880 (2019) 272–280

Contents lists available at ScienceDirect

Journal of Organometallic Chemistry

journal homepage: www.elsevier.com/locate/jorganchem

Synthesis, characterization and chemosensitivity studies of half-sandwich ruthenium, rhodium and iridium complexes containing $\kappa^1_{(S)}$ and $\kappa^2_{(N,S)}$ aroylthiourea ligands

Agreeda Lapasam [a], Omar Hussain [b], Roger M. Phillips [b], Werner Kaminsky [c], Mohan Rao Kollipara [a, *]

[a] Centre for Advanced Studies in Chemistry, North-Eastern Hill University, Shillong, 793022, India
[b] Department of Pharmacy, School of Applied Sciences, University of Huddersfield, Huddersfield, HD1 3DH, UK
[c] Department of Chemistry, University of Washington, Seattle, WA, 98195, USA

ARTICLE INFO

Article history:
Received 20 October 2018
Received in revised form
13 November 2018
Accepted 13 November 2018
Available online 19 November 2018

Keywords:
Ruthenium
Rhodium
Iridium
Thiourea
Chemosensitivity

ABSTRACT

The reaction of $[(p\text{-cymene})RuCl_2]_2$ and $[Cp^*MCl_2]_2$ (M = Rh/Ir) metal precursors with aroylthiourea ligands (L1-L3) yielded a series of neutral mono-dentate complexes **1**–**9**. The neutral mono-dentate coordination of aroylthiourea with metals *via* S atom was confirmed by single crystal X-ray diffraction study. Further reaction of mono-dentate complexes **1**–**9** with excess NaN_3 in polar solvent resulted in the formation of highly strained four member ring $\kappa^2_{(N,S)}$ azido complexes **10**–**18**. Further these complexes were treated with activated alkynes to isolate triazole complexes, but unfortunately the reaction was unsuccessful. All these complexes were fully characterized by various spectroscopic techniques. The molecular structures of the representative complexes have been determined by single crystal X-ray diffraction studies. The molecular structures of the complexes revealed typical piano stool geometry around the metal center. The chemosensitivity activities of the complexes **1**–**9** evaluated against the cancer cell line HCT-116 (human colorectal carcinoma) and ARPE-19 (human retinal epithelial cells) cell line. Of these, complex **3** was the most potent and whilst its potency was less than cisplatin, its selectivity for cancer as opposed to non-cancer cell lines in vitro was comparable to cisplatin.

1. Introduction

The discovery of the anticancer activity of cisplatin by Rosenberg led to the development of numerous metal-based compounds as potential drugs in the war on cancer. Platinum based drugs namely cisplatin, carboplatin and oxaliplatin are among the most effective anticancer drugs, which have been widely used [1,2]. However, some drawback such as neurotoxicity, nephrotoxicity, intrinsic resistance of some tumors and dose-limiting side effects has limited the use of the platinum diammine compounds, cisplatin and carboplatin [3]. In order to overcome these obstacles and develop safer and more effective remedial agents, intensive efforts have been devoted toward the design and pharmacological evaluation of other metal-based drugs [4,5]. In the search for anticancer agents containing metals other than platinum, ruthenium compounds turned out to be the most promising ones, largely because the ligand exchange kinetics of metal complexes in aqueous solution, (which seem to be crucial for the anticancer activity) is favored [6,7]. Ruthenium has therefore been considered to be an attractive alternative to platinum particularly as many ruthenium compounds are not very toxic and some ruthenium compounds have been shown to be quite selective for cancer cells [8,9]. Following the first in vitro study of arene ruthenium compounds as anticancer agents by *Tocher* et al., in 1992, the field of antitumor and anti-metastatic arene ruthenium complexes has received considerable attention and several anticancer ruthenium complexes, NAMI-A and KP1019 exerted potent activities against numerous tumor cells [10,11]. Furthermore, (*p*-cymene)Ru complexes like $[RuCl_2(p\text{-cymene})(pta)]$ (RAPTA-C), show attracted considerable attention due to their promising anti-metastatic activity in vivo activities on the inhibition of metastasis growth, together with a high selectivity and low general toxicity [12]. In addition Cp*rhodium and Cp*iridium complexes have also attracted considerable current interest due to their potential anticancer

* Corresponding author.
E-mail addresses: mohanrao59@gmail.com, kmrao@nehu.ac.in (M.R. Kollipara).

https://doi.org/10.1016/j.jorganchem.2018.11.020
0022-328X/

activity [13–17]. Some of the d^6 metal complexes of ruthenium (II) [18,19], rhodium (III) [17] and iridium (III) [20,21] have also been found to inhibit the tumors by their selective interactions with cellular biomolecules.

Aroylthiourea ligands have been noted for their versatility because they are able to coordinate to a wide range of metal ions as neutral, monobasic or dibasic ligands [22]. N, N-Disubstituted thiourea being versatile precursors has been subjected to a various structural modifications in order to prepare a variety of their derivatives with different biological aspects. Some of N, N-disubstituted thiourea themselves are remarkable owing to their pharmacological and biological importance [23]. In vitro studies have revealed that various classes of thiourea are useful as potential antiviral, antibacterial, antifungal, antitubercular, anti-inflammatory, herbicidal, insecticidal and anticancer agent [24–31]. Thiourea may react with other reagents having different functionalities to yield active compounds of biological significance. The biological importance of both aroylthiourea and the ruthenium-arene unit has prompted us to explore the biological applications of ruthenium-arene complexes containing aroylthiourea ligand. Herein we describe the synthesis of [(*arene*)MCl_2] core complexes containing S donor aroylthiourea ligand and evaluate their cytotoxic properties and non-cancer cells in vitro.

In recent years, we have reported many organometallic complexes including half-sandwich platinum group metal complexes containing thiourea ligands [32–34]. Recently we have also reported the synthesis of strained complexes of arene d^6 metals containing benzoylthiourea ligand [35]. In continuation of our previous work, herein we report the synthesis of neutral monodentate half-sandwich arene ruthenium, rhodium and iridium complexes containing aroylthiourea derivatives and their reactivity with azide. Ligands used in this study are shown in (Chart 1).

2. Experimental section

2.1. Physical methods and materials

The reagents used were of commercial quality and used without further purification. Benzoyl chloride, ammonium thiocyanate, aniline and 4-chloroaniline were purchased from Sigma-Aldrich. 4-Nitroaniline was obtained from Alfa Aesar. The syntheses of all the complexes were performed without using any inert atmosphere. All solvents used for syntheses were dried and distilled prior to use according to standard procedures. Starting compounds [(*p*-cymene)$RuCl_2]_2$ were prepared according to reported method [36], and [$Cp^*MCl_2]_2$ (M = Rh/Ir) complexes were synthesized by using an Anton Paar monowave 50 synthesizer in 10 ml microwave vials equipped with magnetic stirring bars which is described in experimental section. Infrared (IR) spectra (400-4000 cm^{-1}) were recorded on a Perkin-Elmer 983 spectrophotometer with compounds being dispersed as KBr discs. ^1H NMR spectra were recorded on a Bruker Avance II 400 MHz instrument using $CDCl_3$ as solvent chemical shifts were referenced to TMS. Mass spectra were obtained from Waters ZQ 4000 mass spectrometer by ESI method using acetonitrile as solvent. Absorption spectra were recorded on a Perkin-Elmer Lambda 25 UV/Vis spectrophotometer in the range of 200–600 nm at room temperature in acetonitrile. Elemental analyses of the complexes were performed on a Perkin-Elmer 2400 CHN analyzer.

2.2. Single-crystal X-ray structures analyses

The crystal of complexes **2**, **3**, **4**, **5**, **6**, **7**, **8**, **10**, **16** and **17** were obtained by slow diffusion of hexane over dichloromethane solution of the corresponding complexes. Single crystal X-ray diffraction measurement was carried out on an Oxford Diffraction Xcalibur Eos Gemini diffractometer at 293 K using graphite monochromated Mo-Kα radiation (λ = 0.71073 Å). The strategy for the data collection was evaluated using the CrysAlisPro CCD software. Crystal data were collected by standard "phi–omega scan" techniques and were scaled and reduced using CrysAlisPro RED software. The structures were solved by direct methods using SHELXS-97 and refined by full-matrix least squares with SHELXL-97 refining on F2 [37]. The positions of all the atoms were obtained by direct methods. Metal atoms in the complex were located from the E-maps and non-hydrogen atoms were refined anisotropically. The hydrogen atoms bound to the carbon were placed in geometrically constrained positions and refined with isotropic temperature factors, generally 1.2Ueq of their parent atoms. Crystallographic and structure refinement parameters for the complexes are summarized in Table S1 and Table S2, and selected bond lengths and bond angles are presented in Table 1 and Table 2. Figures (1-7) were drawn with ORTEP3 [38].

2.3. Cell line testing

The human colorectal carcinoma cell line HCT116 p53 +/+ cells and the non-cancer human retinal epithelial cell line ARPE-19 were obtained from the American Type Culture Collection. Antiproliferative activity of the compounds was evaluated using the standard MTT (3-(4,5-Dimethylthiazol-2-yl)-2,5-diphenyltetrazolium bromide) cellular viability assay as described elsewhere [39]. Briefly, cells were seeded into 96 well plates at 1.5×10^3 cells per well and incubated for 24 h at 37 °C in an atmosphere of 5% CO_2 prior to drug exposure. Stock solution was freshly prepared by dissolving each of the compounds in dimethylsulphoxide (DMSO) at a concentration of 100 mM, which was subsequently diluted with medium to obtain drug solutions ranging from 0.5 to 100 μM. The final DMSO concentration was 0.1% (v/v), which is nontoxic to cells. Cisplatin was dissolved in phosphate buffered saline at a stock concentration of 25 mM. The cells were exposed to a range of drug concentrations for 96 h and cell survival was determined using the MTT assay. Following drug exposure 20 μL of MTT (0.5 mg/ml) in phosphate buffered saline was added to each well and it was further incubated at 37 °C for 4 h in an atmosphere containing 5% CO_2. The solution was then removed and the formed formazan crystals was dissolved in 150 μM DMSO.

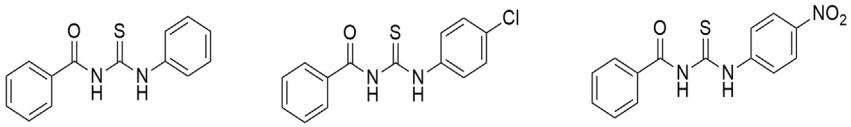

L1 L2 L3

Chart 1. Ligands used in present study.

Table 1
Selected bond lengths (Å) and bond angles (°) of complexes.

Complexes	2	3	4	5	7	8
Bond distances (Å)						
M(1)-CNT	1.787	1.778	1.672	1.689	1.665	1.784
M(1)-Cl(1)	2.413(1)	2.423(1)	2.426(1)	2.440(1)	2.4338(5)	2.4253(9)
M(1)-Cl(2)	2.427(1)	2.410(2)	2.406(1)	2.425(9)	2.4319(7)	2.411(1)
M(1)-S(1)	2.395(1)	2.370(2)	2.418(1)	2.366(1)	2.4004(7)	2.3857(8)
C=S(1)	1.689(9)	1.694(6)	1.703(5)	1.688(3)	1.695(2)	1.691(3)
Bond Angles (°)						
Cl(2)- M(1)-Cl(1)	90.52(4)	88.48(5)	88.87(5)	92.75(3)	87.67(2)	90.55(3)
S(1)- M(1)- Cl(1)	94.09(4)	91.47(5)	89.58(5)	92.34(3)	92.22(2)	92.69(3)
S(1) -M(1)-Cl(2)	92.56(4)	93.735	90.57(5)	92.41(3)	91.28(2)	92.73(3)

Table 2
Selected bond lengths (Å) and bond angles (°) of complexes.

Complexes	10	16	17
Bond distances (Å)			
M(1)-CNT	1.675	1.678	1.784
M(1)-N(1)	2.138(2)	2.152(3)	2.161(3)
M(1)-N (azide)	2.127(4)	2.107(4)	2.125(5)
M(1)-S(1)	2.399(1)	2.406(1)	2.398(2)
C=S	1.713(3)	1.711(4)	1.723(4)
C=O	1.220(4)	1.229(5)	1.240(6)
Bond angle (°)			
N(1)-M(1)-N (azide)	85.7(1)	87.1(1)	90.7(2)
N(1)-M(1)-S(1)	67.27(7)	65.86(9)	67.0(1)
N(azide)-M(1)-S(1)	87.6(1)	88.8(1)	92.4(1)

The absorbance of the resulting solution was recorded at 550 nm using an ELISA spectrophotometer. The percentage of cell survival was calculated by dividing the true absorbance of treated cell by the true absorbance for controls (exposed to 0.1% DMSO). The IC_{50} values were determined from plots of percentage survival against drug concentration. Each experiment was performed in triplicate and a mean value obtained and stated as IC_{50} (μM) ± SD. To compare the response of non-cancer cells to cancer cells, the selectivity index (SI) was also calculated which is defined as the IC_{50} for ARPE-19 cells divided by the IC_{50} for HCT-116 cells. Values ˃1 indicate that complexes have selective activity against cancer compared to non-cancer cells in vitro.

2.4. General procedure for synthesis of ligands (L1-L3)

Freshly prepared benzoyl isothiocyanate was mixed in a 1:1 M ratio with the desired substituted aniline in dry acetone and the mixture was reflux at 50 °C for about 5 h. On cooling, the reaction mixture was slowly poured into acidified (pH 4–5) chilled water and stirred well with a glass rod. The solid, which formed, was separated by filtration and the precipitates were washed with distilled water and dried at room temperature (Scheme 1).

2.5. General preparation of $[Cp^*MCl_2]_2$ (M = Rh/Ir)

$RhCl_3$.$3H_2O$ (0.50 g) or $IrCl_3$.$3H_2O$ (0.50 g) was dissolved in MeOH (3 ml) in a mono-wave vial, and 0.5 ml of 1,2,3,4,5-pentamethylcyclopentadiene was added. The vial was placed in the mono-wave instrument the pressure was set at 20 bar and heated to 110 °C with stirring for 45 min. After cooling to room temperature, the vial was opened. After short vigorous shaking, the precipitate was allowed to settle down, and the solvent was decanted. The microcrystalline product was isolated, washed with diethyl ether (3 × 5 ml), and dried under vacuum. Yield: (88%)

2.6. General procedure for synthesis of neutral complexes (1–9)

A mixture of starting metal precursor (0.1 mmol) and ligands (0.2 mmol) were dissolved in dry methanol (10 ml) and stirred at room temperature for 6 h (Scheme 2). A yellow colored compound precipitated out from the reaction mixture. The precipitate was filtered, washed with cold methanol (5 ml) and diethyl ether (2 × 5 ml) and dried in vacuum.

2.6.1. [(p-cymene)Ru($\kappa^1_{(S)}$-L1)Cl_2] (**1**)

Yield: (68%); IR (KBr, cm^{-1}): 3068–3440 $\nu_{(N-H)}$, 1665 $\nu_{(C=O)}$, 1213 $\nu_{(C=S)}$; ^{1}H NMR (400 MHz, $CDCl_3$, ppm): 12.91 (s, 1H, NH), 11.29 (s, 1H, NH), 8.22 (d, 2H, J = 8 Hz), 7.82 (d, 1H, J = 8 Hz), 7.49 (t, 1H, J = 8 Hz), 7.38–7.45 (m, 5H), 7.32 (t, 1H, J = 8 Hz), 5.33 (d, 2H,

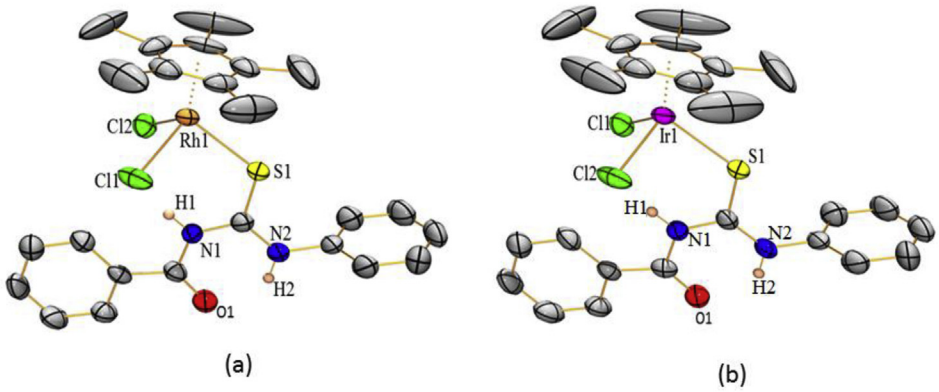

Fig. 1. (a) ORTEP diagram of complex **2** and (b) ORTEP diagram of complex **3** with 50% probability thermal ellipsoids. Hydrogen atoms (except on N) are omitted for clarity.

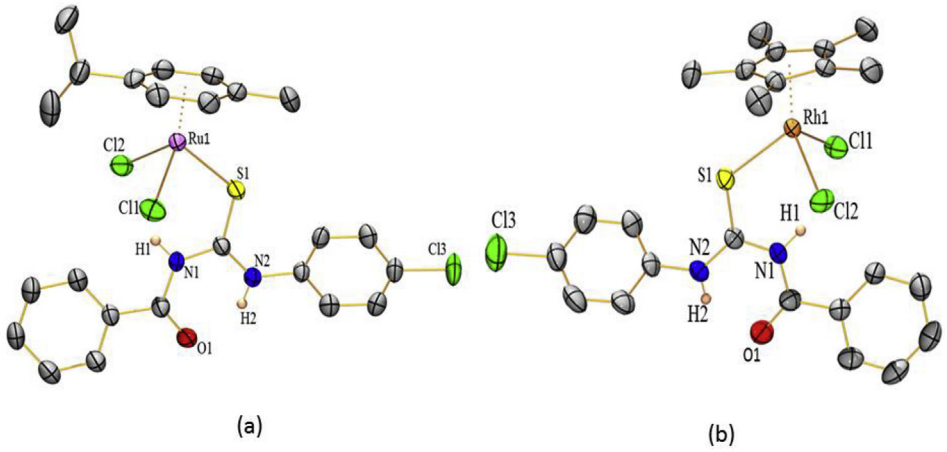

Fig. 2. (a) ORTEP diagram of complex **4** and (b) ORTEP diagram of complex **5** with 50% probability thermal ellipsoids. Hydrogen atoms (except on N) are omitted for clarity.

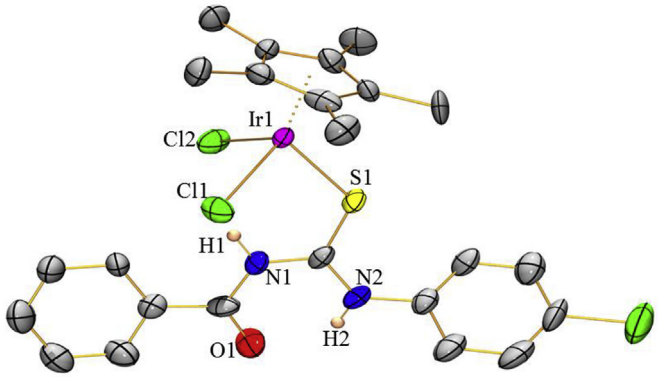

Fig. 3. ORTEP diagram of complex **6** with 50% probability thermal ellipsoids. Hydrogen atoms (except on N) are omitted for clarity. Because of low theta value the crystal structure of complex are presented here to only confirm the structure and composition of molecule.

J = 8 Hz), 5.18 (d, 2H, J = 8 Hz) 2.82–2.93 (sept, 1H), 2.17 (s, 3H), 1.23 (d, 6H, J = 8 Hz); ESI-MS (*m*/*z*): 490.96 $[M-2Cl]^+$; UV-Vis { Acetonitrile, λ_{max} nm ($e/10^{-4}\,M^{-1}\,cm^{-1}$)}: 255 (0.95), 364(0.12). Anal. Calc. for $C_{24}H_{26}Cl_2N_2ORuS$ (562.52): C, 51.24; H, 4.66; N, 4.98. Found: C, 51.30; H, 4.63; N, 4.76.

*2.6.2. [Cp*Rh($\kappa^1_{(S)}$-L1)Cl$_2$](**2**)*

Yield: (72%); IR (KBr, cm^{-1}): 3052–3447 $\nu_{(N-H)}$, 1667 $\nu_{(C=O)}$, 1210 $\nu_{(C=S)}$; ^{1}H NMR (400 MHz, $CDCl_3$, ppm): 13.06 (s, 1H, NH), 11.40 (s, 1H, NH), 8.27 (d, 2H, *J* = 8 Hz), 7.48–7.52 (m, 3H), 7.43 (d, 2H, J = 12 Hz), 7.41 (d, 1H, *J* = 4 Hz), 7.38 (d, 2H, J = 12 Hz), 7.29 (t, 1H, J = 12 Hz), 1.56 (s, 15H). ESI-MS (*m*/*z*): 493.02 $[M-2Cl]^+$; UV-Vis {Acetonitrile, λ_{max} nm ($e/10^{-4}\,M^{-1}\,cm^{-1}$)}: 263 (0.45). Anal. Calc. for $C_{24}H_{27}Cl_2N_2ORhS$ (565.36): C, 50.99; H, 4.81; N, 4.95. Found: C, 51.01; H, 4.75; N, 5.15.

*2.6.3. [Cp*Ir($\kappa^1_{(S)}$-L1)Cl$_2$](**3**)*

Yield: (56%); IR (KBr, cm^{-1}): 3054–3436 $\nu_{(N-H)}$, 1668 $\nu_{(C=O)}$, 1211 $\nu_{(C=S)}$; ^{1}H NMR (400 MHz, $CDCl_3$, ppm): 13.06 (s, 1H, NH),11.84 (s, 1H, NH), 8.41 (d, 2H, J = 8 Hz), 7.60 (t, 1H, J = 8 Hz), 7.51–7.56 (m, 4H), 7.45 (t, 2H, J = 8 Hz), 7.37 (t, 1H, J = 8 Hz), 1.65 (s, 15H); ESI-MS (*m*/*z*): 581.01 $[M-2Cl]^+$; UV-Vis {Acetonitrile, λ_{max} nm ($e/10^{-4}\,M^{-1}\,cm^{-1}$)}: 257(0.30), 350 (0.067). Anal. Calc. for $C_{24}H_{27}Cl_2IrN_2OS$ (654.67): C, 44.03; H, 4.16; N, 4.28. Found: C, 44.01; H, 4.29; N, 4.05.

*2.6.4. [(p-cymene)Ru($\kappa^1_{(S)}$-L2)Cl$_2$](**4**)*

Yield: (73%); IR (KBr, cm^{-1}): 3171–3350 $\nu_{(N-H)}$, 1657 $\nu_{(C=O)}$, 1206 $\nu_{(C=S)}$; ^{1}H NMR (400 MHz, $CDCl_3$, ppm): 12.96 (s, 1H, NH), 11.36 (s, 1H, NH), 8.27 (d, 2H, *J* = 4 Hz), 7.57 (t, 1H, *J* = 8 Hz), 7.50-7.44 (m, 6H), 5.41 (d, 2H, J = 8 Hz), 5.26 (d, 2H, J = 8 Hz), 2.91–2.98 (sept, 1H), 2.24 (s, 3H), 1.30 (d, 6H, J = 8 Hz); ESI-MS (*m*/*z*): $[M-2Cl]^+$;

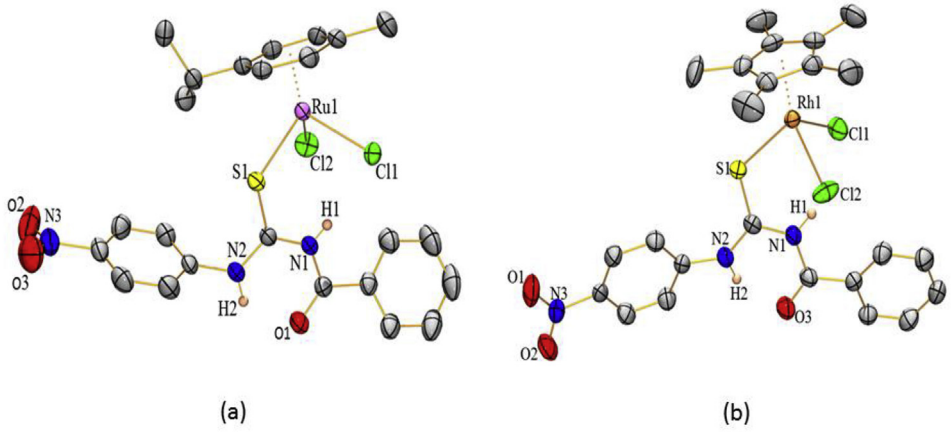

Fig. 4. (a) ORTEP diagram of complex **7** and (b) ORTEP diagram of complex **8** with 50% probability thermal ellipsoids. Hydrogen atoms (except on N) are omitted for clarity.

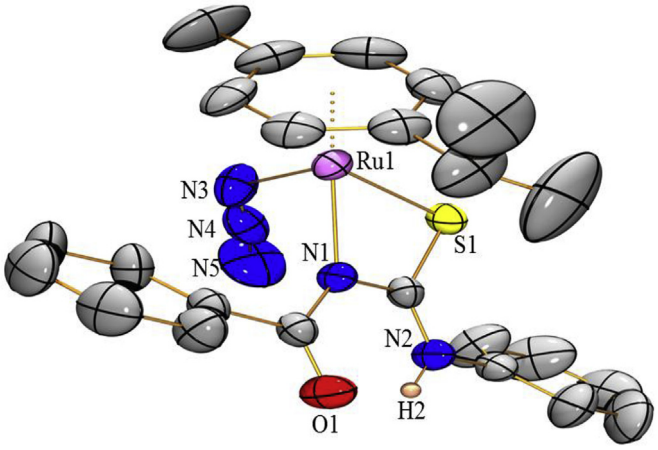

Fig. 5. ORTEP diagram of complex **10** with 50% probability thermal ellipsoids. Hydrogen atoms (except on N) are omitted for clarity.

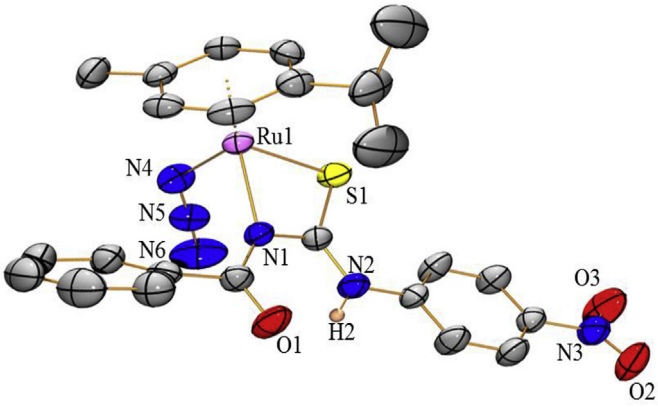

Fig. 6. ORTEP diagram of complex **16** with 50% probability thermal ellipsoids. Hydrogen atoms (except on N) are omitted for clarity.

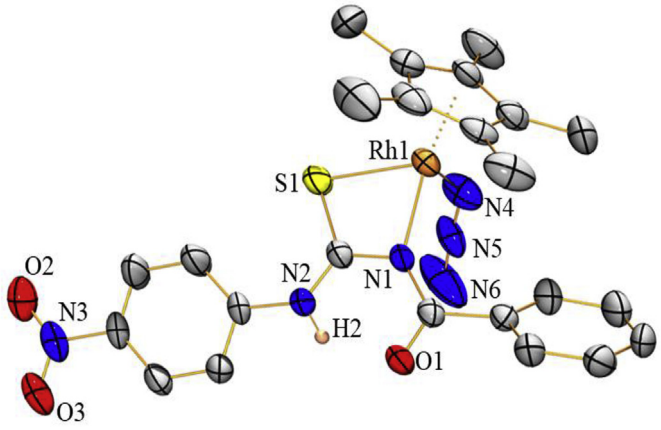

Fig. 7. ORTEP diagram of complex **17** with 50% probability thermal ellipsoids. Hydrogen atoms (except on N) are omitted for clarity. Because of low theta value the crystal structure of complex are presented here to only confirm the structure and composition of molecule.

UV-Vis {Acetonitrile, λ_{max} nm ($e/10^{-4}\,M^{-1}\,cm^{-1}$)}: 260 (0.73), 357 (0.10). Anal. Calc. for $C_{24}H_{25}Cl_3N_2ORuS$ (596.96): C, 48.29; H, 4.22; N, 4.69. Found: C, 48.33; H, 4.22; N, 4.77.

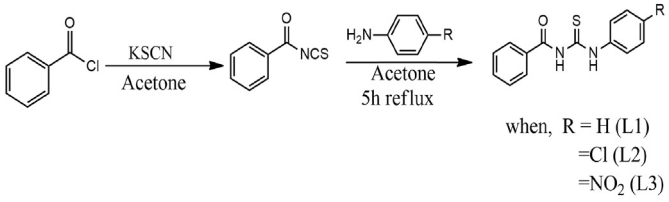

Scheme 1. Synthesis of thiourea ligands (**L1-L3**).

*2.6.5. [Cp*Rh($\kappa^1_{(S)}$-L2)Cl_2] (**5**)*

Yield: (81%); IR (KBr, cm^{-1}): 3128–3434 $\nu_{(N-H)}$, 1665 $\nu_{(C=O)}$, 1211 $\nu_{(C=S)}$; ^{1}H NMR (400 MHz, $CDCl_3$, ppm): 13.10 (s, 1H, NH), 11.50 (s, 1H, NH), 8.34 (d, 2H, $J = 8$ Hz), 7.58 (t, 1H, $J = 8$ Hz), 7.49–7.53 (m, 4H, $J = 8$ Hz), 7.43 (d, 2H, $J = 8$ Hz), 1.75 (s, 15H); ESI-MS (m/z): 527.19 $[M - 2Cl]^+$; UV-Vis {Acetonitrile, λ_{max} nm ($e/10^{-4}\,M^{-1}\,cm^{-1}$)}: 264 (0.38). Anal. Calc. for $C_{24}H_{26}Cl_3N_2ORhS$ (599.81): C, 48.06; H, 4.37; N, 4.67. Found: C, 47.85; H, 4.42; N, 4.45.

*2.6.6. [Cp*Ir($\kappa^1_{(S)}$-L2)Cl_2] (**6**)*

Yield: (73%); IR (KBr, cm^{-1}): 3056–3430 $\nu_{(N-H)}$, 1669 $\nu_{(C=O)}$, 1204 $\nu_{(C=S)}$; ^{1}H NMR (400 MHz, $CDCl_3$, ppm): 13.06 (s, 1H, NH), 11.88 (s, 1H, NH), 8.40 (d, 2H, $J = 8$ Hz), 7.60 (t, 1H, $J = 8$ Hz), 7.47–7.55 (m, $J = 8$ Hz, 4H), 7.44 (dd, 2H, $J = 8$ Hz), 1.61 (s, 15H); (m/z) ESI-MS: 617.22 $[M - 2Cl]^+$; UV-Vis {Acetonitrile, λ_{max} nm ($e/10^{-4}\,M^{-1}\,cm^{-1}$)}: 271(0.83), 355 (0.078). Anal. Calc. for $C_{24}H_{26}Cl_3IrN_2OS$ (689.12): C, 41.83; H, 3.80; N, 4.07. Found: C, 41.84; H, 3.82; N, 4.15.

*2.6.7. [(p-cymene)Ru($\kappa^1_{(S)}$-L3)Cl_2] (**7**)*

Yield: (84%); IR (KBr, cm^{-1}): 3164–3467 $\nu_{(N-H)}$, 1659 $\nu_{(C=O)}$, 1209 $\nu_{(C=S)}$; ^{1}H NMR (400 MHz, $CDCl_3$, ppm): 13.41 (s, 1H, NH), 11.49 (s, 1H, NH), 8.35 (d, 2H, $J = 8$ Hz), 8.27 (d, 2H, J = 8 Hz), 7.77 (d, 2H, $J = 8$ Hz), 7.58 (t, 1H, J = 4 Hz), 7.50 (t, 2H, $J = 8$ Hz), 5.45 (d, 2H, $J = 8$ Hz), 5.30 (d, 2H, J = 8 Hz), 2.91–3.02 (sept, 1H), 2.27 (s, 3H), 1.31 (d, 6H); ESI-MS (m/z): 535.13 $[M - 2Cl]^+$; UV-Vis {Acetonitrile, λ_{max} nm ($e/10^{-4}\,M^{-1}\,cm^{-1}$)}: 281 (0.40), 347 (0.22). Anal. Calc. for $C_{24}H_{25}Cl_2N_3O_3RuS$ (607.51): C, 47.45; H, 4.15; N, 6.92. Found: C, 47.43; H, 4.16; N, 6.74.

*2.6.8. [Cp*Rh($\kappa^1_{(S)}$-L3)Cl_2] (**8**)*

Yield: (75%); IR (KBr, cm^{-1}): 3238–3435 $\nu_{(N-H)}$, 1671 $\nu_{(C=O)}$, 1206 $\nu_{(C=S)}$; ^{1}H NMR (400 MHz, $CDCl_3$, ppm): 13.48 (s, 1H, NH), 11.55 (s, 1H, NH), 8.27 (d, 4H, $J = 8$ Hz), 7.75 (d, 2H, $J = 8$ Hz), 7.53 (t, 1H, $J = 8$ Hz), 7.41 (t, 2H, $J = 8$ Hz), 1.59 (s, 15H); ESI-MS (m/z): 538.08 $[M - 2Cl]^+$; UV-Vis {Acetonitrile, λ_{max} nm ($e/10^{-4}\,M^{-1}\,cm^{-1}$)}: 259 (1.71). Anal. Calc. for $C_{24}H_{26}Cl_2N_3O_3RhS$ (610.36): C, 47.23; H, 4.29; N, 6.88. Found: C, 47.25; H, 4.30; N, 6.74.

*2.6.9. [Cp*Ir($\kappa^1_{(S)}$-L3)Cl_2] (**9**)*

Yield: (79%); IR (KBr, cm-^{1}): 3241–3447 $\nu_{(N-H)}$, 1671 $\nu_{(C=O)}$, 1210 $\nu_{(C=S)}$; ^{1}H NMR (400 MHz, $CDCl_3$, ppm): 13.53 (s, 1H, NH), 12.03 (s, 1H, NH), 8.42 (d, 2H, $J = 4$ Hz), 8.34 (d, 2H, $J = 8$ Hz), 7.80 (d, 2H, $J = 4$ Hz), 7.63 (t, 1H, $J = 8$ Hz), 7.55 (t, 2H, J = 8 Hz), 1.64 (s, 15H); ESI-MS (m/z): 626.14 $[M - 2Cl]^+$; UV-Vis {Acetonitrile, λ_{max} nm ($e/10^{-4}\,M^{-1}\,cm^{-1}$)}: 275 (1.11), 345 (0.22). Anal. Calc. for $C_{24}H_{26}Cl_2IrN_3O_3S$ (699.67): C, 41.20; H, 3.75; N, 6.01. Found: C, 41.19; H, 3.78; N, 6.17.

2.7. General procedure for synthesis of azido complexes (10–18)

For the synthesis of azido complexes **10**–**18** these two reaction routes are possible-:

Route a: A suspension of the corresponding starting complexes

1–**9** and NaN_3 in 1:5 M ratios was suspended in dry methanol (10 ml) and stirred at room temperature for 8 h (Scheme 3). The solvent was removed to dryness using rotary evaporator. The residue was extracted with dichloromethane, filtered and precipitated with hexane. This accounts for the higher yield of complexes by this route as compared to that obtained by the other route (route b).

Route b: In addition, the terminal azido complexes **10, 13, 16** have also been prepared by treatment of azido dimer [(p-cymene) $Ru(\mu\text{-}N_3)Cl]_2$ with Ligands **L1**-**L3** in dry methanol. The resulting mixture was stirred for 8 h at room temperature. After completion of the reaction, the solvent was removed to dryness using rotary evaporator the expected complex was extracted with dichloromethane, filtered, precipitated with hexane and dried in vacuum.

*2.7.1. [(p-cymene)Ru($\kappa^2_{(N,S)}$-L1)N_3] (**10**)*

Yield: (68%); IR (KBr, cm^{-1}): 3433 $\nu_{(N\text{-}H)}$, 2030 $\nu_{(N3)}$, 1617 $\nu_{(C=O)}$, 1192 $\nu_{(C=S)}$; ^1H NMR (400 MHz, $CDCl_3$, ppm): 12.54 (s, 1H), 8.04 (d, 2H, J = 8 Hz), 7.51–7.58 (m, 5H), 7.40 (t, 2H, J = 8 Hz), 7.28 (d, 1H, J = 8 Hz), 5.24 (d, 1H, J = 4 Hz), 4.67 (d, 1H, J = 4 Hz), 4.62 (d, 1H, J = 4 Hz), 4.46 (d, 1H, J = 8 Hz), 2.60–2.70 (sept, 1H), 2.09 (s, 3H), 1.20 (d, 6H, J = 8 Hz). ^{13}C NMR (100 MHz,$CDCl_3$, ppm): 186.06, 178.67, 137.58, 135.40, 131.14, 129.20, 128.07, 123.82, 100.86, 100.28, 83.90, 83.11, 80.40, 78.57, 31.27, 23.26, 21.76, 18.02; UV-Vis {Acetonitrile, λ_{max} nm ($e/10^{-4}\,M^{-1}\,cm^{-1}$)}: 284 (0.75), 422 (0.18).

*2.7.2. [Cp*Rh($\kappa^2_{(N,S)}$-L1)N_3] (**11**)*

Yield: (68%); IR (KBr, cm^{-1}): 3436 $\nu_{(N\text{-}H)}$, 2034 $\nu_{(N3)}$, 1627 $\nu_{(C=O)}$, 1191$\nu_{(C=S)}$; ^1H NMR (400 MHz, $CDCl_3$, ppm): 12.74 (s, 1H), 8.21 (d, 2H, J = 8 Hz), 7.55 (t, 3H, J = 8 Hz), 7.47–7.52 (m, 3H), 7.40 (t, 3H, J = 8 Hz), 1.41 (s, 15H); ESI-MS (*m/z*): 493.16 $[M - N_3]^+$. UV-Vis {Acetonitrile, λ_{max} nm ($e/10^{-4}\,M^{-1}\,cm^{-1}$)}: 293 (0.85), 422 (0.18). Anal. Calc. for $C_{24}H_{26}N_5ORhS$ (535.97): C, 53.83; H, 4.89; N, 13.08. Found: C, 53.87; H, 4.82; N, 13.11.

*2.7.3. [Cp*Ir($\kappa^2_{(N,S)}$-L1)N_3] (**12**)*

Yield: (56%); IR (KBr, cm^{-1}): 3420$\nu_{(N\text{-}H)}$, 2036 $\nu_{(N3)}$, 1618 $\nu_{(C=O)}$, 1198 $\nu_{(C=S)}$; ^1H NMR (400 MHz, $CDCl_3$, ppm): 12.75 (s, 1H), 8.22 (d, 1H, J = 8 Hz), 8.10 (d, 1H, J = 8 Hz), 7.57 (d, 1H, J = 8 Hz), 7.48 (t, 3H, J = 4 Hz), 7.40 (d, 2H, J = 4 Hz), 7.33 (d, 1H, J = 4 Hz), 1.65 (s, 15H)· ^{13}C NMR (100 MHz,$CDCl_3$, ppm): 173.44, 167.77, 145.68, 139.88, 130.33, 129.59, 127.42, 125.25, 126.25, 89.45, 9.02; ESI-MS (*m/z*): 582.80 $[M - N_3]^+$. UV-Vis {Acetonitrile, λ_{max} nm ($e/10^{-4}\,M^{-1}\,cm^{-1}$)}: 204 (0.832), 361 (0.41).

*2.7.4. [(p-cymene)Ru($\kappa^2_{(N,S)}$-L2)N_3] (**13**)*

Yield: (71%); IR (KBr, cm^{-1}): 3433 $\nu_{(N\text{-}H)}$, 2030 $\nu_{(N3)}$, 1611 $\nu_{(C=O)}$, 1193 $\nu_{(C=S)}$; ^1H NMR (400 MHz, $CDCl_3$, ppm): 12.50 (s, 1H), 8.02 (d, 2H, J = 4 Hz), 7.51–7.58 (m, 3H), 7.46 (d, 2H, J = 8 Hz), 7.35 (d, 2H, J = 12 Hz), 5.25 (d, 1H, J = 8 Hz), 4.67 (d, 1H, J = 4 Hz), 4.62 (d, 1H, J = 4 Hz), 4.46 (d, 1H, J = 4 Hz), 2.59–2.69 (sept, 1H), 2.08 (s, 3H), 1.19 (d, 6H); ^{13}C NMR (100 MHz,$CDCl_3$, ppm): 189.13, 178.67, 131.97, 129.33, 129.02, 128.79, 128.08, 127.18, 125.17, 121.57, 99.67, 97.27, 83.82, 81.96, 80.10, 31.28, 30.18, 22.31, 17.52; UV-Vis {Acetonitrile, λ_{max} nm ($e/10^{-4}\,M^{-1}\,cm^{-1}$)}: 277 (0.92), 443 (0.16).

*2.7.5. [Cp*Rh($\kappa^2_{(N,S)}$-L2)N_3] (**14**)*

Yield: (65%); IR (KBr, cm^{-1}): 3423 $\nu_{(N\text{-}H)}$, 2037 $\nu_{(N3)}$, 1621 $\nu_{(C=O)}$, 1190 $\nu_{(C=S)}$; ^1H NMR (400 MHz, $CDCl_3$, ppm): 12.72 (s, 1H), 8.20 (d, 2H, J = 8 Hz), 7.49–7.52 (m, 5H), 7.35 (d, 2H, J = 12 Hz), 1.41 (s, 15H); ^{13}C NMR (100 MHz,$CDCl_3$, ppm): 186.76, 176.69, 134.59, 134.35, 131.92, 131.66, 129.28, 128.94, 127.61, 127.18, 93.15, 8.72; UV-Vis {Acetonitrile, λ_{max} nm ($e/10^{-4}\,M^{-1}\,cm^{-1}$)}: 265 (0.90), 430 (0.17). Anal. Calc. for $C_{24}H_{25}ClN_5ORhS$ (569.91): C, 50.58; H, 4.42; N, 12.29. Found: C, 50.65; H, 4.45; N, 12.18.

*2.7.6. [Cp*Ir($\kappa^2_{(N,S)}$-L3)N_3] (**15**)*

Yield: (54%); IR (KBr, cm^{-1}): 3402 $\nu_{(N\text{-}H)}$, 2037 $\nu_{(N3)}$, 1619 $\nu_{(C=O)}$, 1194$\nu_{(C=S)}$; ^1H NMR (400 MHz, $CDCl_3$, ppm): 8.04 (d, 2H, J = 8 Hz), 7.47 (d, 2H, J = 8 Hz), 7.37 (t, 3H, J = 8 Hz), 6.59 (d, 2H, J = 12 Hz), 1.68 (s, 15H); ESI-MS (*m/z*): 612.96 $[M - N_3]^+$.UV-Vis {Acetonitrile, λ_{max} nm ($e/10^{-4}\,M^{-1}\,cm^{-1}$)}: 257 (0.59), 361(0.22).

*2.7.7. [(p-cymene)Ru($\kappa^2_{(N,S)}$-L3)N_3] (**16**)*

Yield: (69%); IR (KBr, cm^{-1}): 3432 $\nu_{(N\text{-}H)}$, 2035 $\nu_{(N3)}$, 1627 $\nu_{(C=O)}$, 1189 $\nu_{(C=S)}$; ^1H NMR (400 MHz, $CDCl_3$, ppm):12.98 (s, 1H), 8.26 (d, 2H, J = 8 Hz), 8.03 (d, 2H, J = 8 Hz), 7.76 (d, 2H, J = 8 Hz), 7.53–7.62 (m, 3H), 5.30 (d, 1H, J = 8 Hz), 4.72 (d, 1H, J = 8 Hz), 4.66 (d, 1H, J = 8 Hz), 4.50 (d, 1H, J = 4 Hz), 2.61–2.71 (sept, 1H), 2.10 (s, 3H), 1.21 (d, 6H, J = 8 Hz); ESI-MS (*m/z*): 536.08 $[M - N_3]^+$. UV-Vis {Acetonitrile, λ_{max} nm ($e/10^{-4}\,M^{-1}\,cm^{-1}$)}: 278(1.16), 339 (0.68). Anal. Calc. for $C_{24}H_{24}N_6O_3RuS$ (577.62): C, 49.90; H, 4.19; N, 14.55. Found: C, 49.89; H, 4.23; N, 14.68.

*2.7.8. [Cp*Rh($\kappa^2_{(N,S)}$-L3)N_3] (**17**)*

Yield: (58%); IR (KBr, cm^{-1}): 3428 $\nu_{(N\text{-}H)}$, 2034 $\nu_{(N3)}$, 1614 $\nu_{(C=O)}$, 1193 $\nu_{(C=S)}$; ^1H NMR (400 MHz, $CDCl_3$, ppm): 13.13 (s, 1H), 8.20 (d, 2H, J = 8 Hz), 8.13 (d, 2H, J = 8 Hz), 7.73 (d, 2H, J = 8 Hz), 7.49 (t, 1H, J = 8 Hz), 7.43 (t, 1H, J = 8 Hz), 1.36 (s, 15H); ESI-MS (*m/z*): 537.08 $[M - N_3]^+$. UV-Vis {Acetonitrile, λ_{max} nm ($e/10^{-4}\,M^{-1}\,cm^{-1}$)}: 269 (0.96), 338 (0.68), 432 (0.16).

*2.7.9. [Cp*Rh($\kappa^2_{(N,S)}$-L3)N_3] (**18**)*

Yield: (62%); IR (KBr, cm^{-1}): 3432 $\nu_{(N\text{-}H)}$, 2030 $\nu_{(N3)}$, 1627 $\nu_{(C=O)}$, 1202$\nu_{(C=S)}$; ^1H NMR (400 MHz, $CDCl_3$, ppm): 8.39 (d, 1H, J = 8 Hz), 7.96 (d, 1H, J = 8 Hz), 7.83 (d, 1H, J = 8 Hz), 7.71 (d, 2H, J = 8 Hz), 7.50 (d, 2H, J = 8 Hz), 7.37 (t, 2H, J = 8 Hz), 1.74 (s, 15H); ESI-MS (*m/z*): 628.14 $[M - N_3]^+$. UV-Vis {Acetonitrile, λ_{max} nm ($e/10^{-4}\,M^{-1}\,cm^{-1}$)}: 281 (0.44), 344 (0.30).

3. Results and discussion

3.1. Synthesis of complexes

The metal complexes **1**–**9** were synthesized by the reaction of Ru, Rh and Ir metal precursors with the thiourea ligands **L1**-**L3** in methanol and are represented in (Scheme 2). All these metal complexes were obtained in good yield and are yellow or red in color. They are stable in air as well as in solid state, and are non-hygroscopic. These complexes were isolated as neutral complexes with mono-dentate $\kappa^1_{(S)}$ coordination. Azido compounds were synthesized by the substitution of the chloride ligand by azide group following two routes. Treatment of half-sandwich mononuclear complexes **1**–**9** with five fold of NaN_3 in methanol (Scheme 3) resulted in the substitution of the chloride ligand and the formation of highly strained four membered chelated $\kappa^2_{(N,S)}$ azido complexes **10**–**18** (Scheme 3 route a). Similarly, these terminal

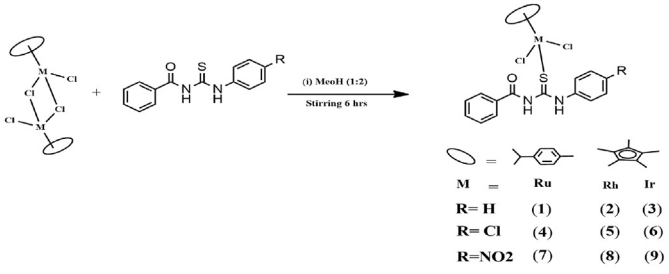

Scheme 2. Schematic representation for the synthesis of complexes (1–9).

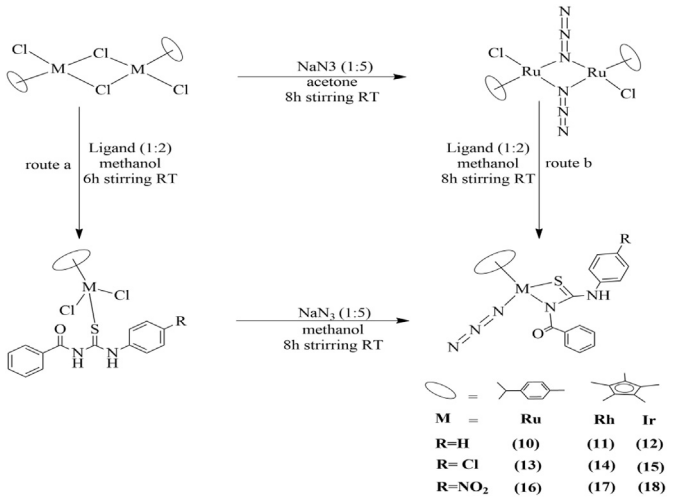

Scheme 3. Schematic representation for the synthesis of complexes (**10**–**18**).

azido complexes **10**, **13**, and **16** can be prepared from the binuclear *p*-cymene ruthenium azido complexes $[(p\text{-cymene})Ru(\mu\text{-}N_3)Cl]_2$ by reacting with ligand L1-L3 in methanol (route b). However, 'route a' is more preferable than 'route b' as it gives higher percentage yield of the expected complex, hence we reported the yield obtained through this route in the experimental section. Our effort to make triazole complexes by reaction of terminal azido complexes with excess of dimethylacetylenedicarboxylate ($MeO_2CC_2CO_2Me$) or diethylacetylenedicarboxylate ($EtO_2CC_2CO_2Et$) in dichloromethane was unsuccessful. Further we have carried out the antibacterial studies for ligands and complexes against four pathogenic bacteria *viz., S. aureus, E. coli*, *B. thuringiensis* and *P. aeruginosa* but none of the compounds showed any activity. All the synthesized complexes are soluble in common organic solvents such as dichloromethane, acetonitrile and acetone but insoluble in diethyl ether and hexane. All the synthesized ligands and complexes were fully characterized by various spectroscopic techniques.

3.2. Spectroscopic characterization of complexes

The IR spectra of free aroyl thiourea ligands showed characteristic stretching frequencies at 3076–3312 cm^{-1} corresponding to $\nu_{(N-H)}$ which also present in the same region in all the complexes indicating that deprotonation does not occur. A strong band observed in the region 1657–1661 cm^{-1} in the FT-IR spectra of the ligands was assigned to the $\nu_{(C=O)}$, the stretching vibration $\nu_{(C=O)}$ bands remain unaltered upon complexation indicating non participation of carbonyl oxygen in coordination. The characteristic band for $\nu_{(C=S)}$ appeared at 1232–1241 cm^{-1} in the spectra of L1-L3 was shifted to lower frequency (1189–1213 cm^{-1}) on complexation indicating involvement of sulfur in coordination to the metal center.

The IR spectra of the azido complexes **10**–**18** showed sharp absorption band at frequencies 2030–2037 cm^{-1} corresponding to terminal υ_{N3}. When synthesis *via* route b the IR spectra of these complexes also show absence of the bridging azido band at 2065 cm^{-1} and the appearance of new bands for terminal azido group in the above mentioned range. This leads us to infer the formation of terminal azido complexes.

The ^{1}H NMR spectra of the complexes **1**–**9** (Figs. S1–S8) show a downfield shift in protons of ligand after forming complexes, which is due to the deshielding effect exerted by metal on the ligands. The ^{1}H NMR of the complexes **1**–**9** show two singlet around 13.53-12.96 and 11.88-11.29 which is attributed to the N-H proton signals of thiocarbonyl and carbonyl attached N-H respectively. The appearance of two N-H signals in all the complexes indicates that the N-H group is not involved in bonding. Resonances due to the aromatic ligands protons were all in the expected range of 8.29-7.21 ppm, which indicates the coordination of the thiourea ligand to the metal center. In addition to the signals for the ligand protons, a sharp singlet was observed for all the rhodium and iridium complexes between 1.58 and 1.63 ppm corresponding to the methyl protons of the Cp* ring. The ^{1}H NMR spectra of complexes **1**, **4** and **7** displays a doublet for methyl protons of isopropyl group at 1.23 ppm, 1.30 ppm and 1.31 ppm respectively, a singlet at 2.17 ppm, 2.24 ppm and 2.27 ppm for methyl group, a septet at 2.86 ppm, 2.94 ppm and 2.96 ppm for one proton of isopropyl group of p-cymene moiety. Two doublets were observed in the range 5.18 ppm–5.45 ppm corresponds to the aromatic protons of *p*-cymene.

The ^{1}H NMR spectra of all the azido complexes **10**–**18** (Figs. S9–S16) show the disappearance of one N–H proton, which strongly supports the deprotonation of one amido hydrogen and this has also been confirmed from molecular structures. The deprotonation of amido hydrogen (NH) resulted in the generation of negative charge on amido nitrogen atom, which leads to the formation of neutral complexes **10**–**18**. The azido complexes show a singlet around 12.50–13.13, which is attributed to one N-H proton signals. The appearance of one N-H signal in all the complexes indicates that only one N-H group involved in bonding. Resonances due to the aromatic ligands protons were all in the same range of 8.40-7.27 ppm. The rhodium and iridium complexes displayed only one singlet for the methyl protons of the Cp* group around 1.52–1.75 ppm. The binding of the azide ligand to the ruthenium atom in mononuclear ruthenium complexes leads to the splitting of the *p*-cymene ring protons upon coordination of the ligand to the *p*-cymene moiety. The signals associated with the *p*-cymene ring protons consisted of four doublets around 5.29–4.50 ppm. This unexpected pattern of signals for the *p*-cymene ligand is consisted with the metal center being chiral upon coordination of the azide ligand and these results correlates well with similar reported complexes [35]. In addition the methine and methyl protons of the *p*-cymene group exhibited septet around 2.65 ppm and singlet around 2.09 ppm.

The ^{13}C NMR spectra of the complexes further justify the coordination of the ligands and formation of complexes. The ^{13}C NMR spectra of the representative complexes are provided in the supplementary information (Figs. S29–S31). The ^{13}C NMR spectra of the complexes displayed signals associated with the ligand carbons, *p*-cymene ligand carbons, methyl carbon of Cp* and ring carbon of Cp*. The carbon resonance of the thiocarbonyl (C=S) group appeared in the lower frequency region around 173.44–186.76 ppm and the carbonyl (C=O) group appeared in the range of 178.67 to 167.77 ppm. The aromatic carbons signals for the ligands were observed in the range of 121.57–145.68 ppm. The methyl, methine and isopropyl carbon resonances of the *p*-cymene ligand were observed in the region around 17.52–31.28 ppm. The signals associated with the ring carbons of the Cp* ligand was observed in the region 89.45–93.15 ppm in contrast the methyl carbon resonances was observed as a sharp peak at 8.72 and 9.02 ppm. Overall results from the NMR spectral studies strongly support the formation of the metal complexes.

The mass spectra of the complexes are presented in the Supplementary Information Figs. S17–S28. Complexes display their predominant molecular ion peaks at *m*/*z*: 490.96, 493.02, 581.01, 524.23, 527.19, 617.22, 535.13, 538.08 and 659.12 respectively which correspond to $[M-2Cl]^+$ ion peak. Complexes 11, 12, 15, 16, 17, and 18 display their predominant peaks at *m*/*z*: 493.16, 582.80,

616.96, 536.08, 537.08, and 628.14 respectively which correspond to $[M - N_3]^+$. The appearance of these peaks in its mass spectra clearly indicates the formation of thiourea metal complexes. The peaks corresponding to the loss of the thiourea ligands as well as the arene ring are not observed which indicates the strong metal to ligand and metal to arene bond. The mass spectral values strongly justify the composition and formation of these complexes.

The electronic spectra of the complexes were recorded in acetonitrile at 10^{-4} M concentration at room temperature. The electronic spectra of complexes display two absorption band in the higher energy region around 230–340 nm (Figs. S32–33). The band in the range of 230–280 nm can be assigned as π-π* and n-π * transition. The band in the lower energy region around 345–405 nm can be assigned as metal (dπ) to π* ligand charge transfer (MLCT).

3.3. Description of the molecular structures of complexes

The molecular structure of the complexes along with the crystallographic numbering schemes is depicted in the Figs. 1–7. Because of low theta value the crystal structures of complexes **6** and **17** are presented here to only confirm the structure and composition of molecule. The summary of the crystal data, data collection and structure refinement parameters are summarized in Table S1 and Table S2. Selected bond lengths, bond angles and metal atom involving ring centroid values are listed in Tables 1 and 2. The crystals of the complexes **2, 3, 4, 5, 6, 7, 8, 10**, **16** and **17** suitable for X-ray diffraction study were obtained by slow diffusion of hexane to the concentrated dichloromethane solutions of the compound. By carrying out the single crystal analyses we were able to confirm the variety of bonding modes associated with the ligand. The complexes adopted a piano-stool geometry, where *p*-cymene and Cp* moiety served as the top of the stool and the three leg sites were occupied by sulfur from ligands and two terminal chlorides. The metal atom in these complexes is situated in a pseudo-octahedral arrangement with the ligand coordinating through the sulfur atom. In complexes **1**–**9** the thiourea ligands acted as a neutral mono-dentate ligand coordinating metal *via* S atom.

Complexes **2**, **3, 5** and **8** crystallized in monoclinic with space group $P2_1/c$. Complex **4** crystallized in monoclinic system with space group *C2/c*, whereas Complex **7** crystallized in triclinic system with space group *P 1*. The distance between the metal M to centroid of the *p*-cymene/Cp* ring are {1.787 (**2**), 1.778 (**3**), 1.672 (**4**), 1.689 (**5**), 1.665 (**7**), 1.784 (**8**) Å}. The metal to sulfur bond distances of complexes **2**, **3**, **4**, **5, 7** and **8** were found to be 2.395(1), 2.370(2), 2.418(1), 2.366(1), 2.4004(7) and 2.3857 (8) respectively, whereas the M-Cl1 bond distances of complexes **2**, **3**, **4**, **5, 7** and **8** were found to be 2.413(1), 2.423(1), 2.426(1), 2.440(1), 2.4338(5) and 2.4253(9) and the M-Cl2 bond distances were found to be 2.427(1), 2.410 (2), 2.406 (1), 2.425 (1), 2.4319 (7) and 2.411 (1) respectively which are comparable with earlier reported complexes [34]. The C-S bond length in these complexes lie in the range 1.688–1.703 Å which are in good agreement with other related compounds for a C=S double bond [40]. The bond angle values S-M-Cl and Cl-M-Cl are found to be in the range 87.67–94.09° thus suggesting the pseudo octahedral arrangement around the metal center.

Further reaction of the mono-dentate thiourea *p*-cymene ruthenium, Cp* rhodium and Cp* iridium complexes with excess of sodium azide resulted in deprotonation of the amido hydrogen which changed the bonding behavior of the thiourea ligand towards both *p*-cymene ruthenium and Cp* rhodium complexes as confirmed from the molecular structures. X-ray studies of these complexes revealed that upon coordination of azide group to the metal it cause deprotonation of amido N-H and the bonding of the thiourea derivatives were altered. All the thiourea derivatives revealed interesting coordination towards metal upon coordination of the azide group. The *p*-cymene ruthenium azido complexes **10** and **16** crystallized in monoclinic system with space group *P 21/c* and *P21/n* respectively. Whereas the Cp*rhodium azido complex **17** crystallized in monoclinic system with space group $P2_1/n$. The deprotonation of the amido hydrogen (NH) forced the thiourea ligand to coordinate metal in an anionic bidentate chelating fashion via S and N thus forming a highly strained four membered chelated ring and the oxidation state of metal is balanced by the amido group nitrogen and azide nitrogen. The distance between the metal M to centroid of the *p*-cymene/Cp* ring in complexes **10, 16** and **17** are 1.675, 1.678 and 1.784 Å [41]. The metal to sulfur bond distance of complex **16** is 2.406(1) was found to be slightly longer than complex **17** 2.398(2) Å whereas the metal to azide bond distance are 2.107(4) and 2.125(5) Å respectively. The C=S bond length in complex **17** is 1.723(4) Å was slightly longer than that in complex **16** 1.711(4) Å. The bond angle values N-M-N and N-M-S for complexes **10**, **16** and **17** are given in Table 2. The bite angle of complexes **10, 16** and **17** are 67.27°, 65.86° and 67° respectively which is the strain angle giving a pseudo-octahedral arrangement of piano stool half sandwich complex.

Furthermore, the crystal structure of complex **3** display two different types of interaction intramolecular and intermolecular hydrogen bonding; the first interaction is N-H···O between the carbonyl oxygen and amido H-atom (1.907 Å), and the N-H···Cl between the other amido hydrogen and Cl-atom attached to iridium metal (2.424 Å). The second is C-H···π interaction between the benzoyl moiety and the H-atom of aniline (3.517 Å) (Fig. S34). Similarly the crystal structure of complex **16** exhibits N-H···O interaction between the carbonyl oxygen and amido H-atom (1.902 Å), the C-H···N interaction between the H-atom of *p*-cymene and azide nitrogen (2.758 Å), and C-H···O interaction between the H-atom of *p*-cymene and O-atom of nitro group (2.415 Å) (Fig. S35).

3.4. Chemosensitivity studies

The complexes (**1**–**9**) were tested for their cytotoxicity against cancer cell line HCT-116 (human colon carcinoma) and non-cancer cell line ARPE-19 (human retinal epithelial cells). The response of the cell lines HCT-116 and ARPE-19 (human retinal epithelial cells) to the test complexes **1**–**9** and cisplatin is presented in tabular form in Table 3. Complexes **5**, **6**, and **8** were found to be inactive against both the cell line with IC_{50} values > 100 μM. Complexes **1**, **2**, **7** and **9** were found to be less active against HCT-116 cell line. In contrast complexes **3** and **4** displayed moderate activity against both cell lines with IC_{50} value of 35.172 ± 1.175 and 43.751 ± 2.480 μM. Of the

Table 3
Response of HCT-116 (human colon cancer) and ARPE-19 to complexes **1**–**9** and cisplatin. Each IC_{50} value represents the mean ± standard deviation from three independent experiments. The IC_{50} selectivity index is defined as the mean IC_{50} for ARPE-19 cells divided by the mean IC_{50} for HCT-116 cells with values greater than 1 representing selective cell kill in cancer cells compared to non-cancer cells.

Compounds	IC_{50} (μM)		
	HCT-116	ARPE-19	Selectivity Index
Complex **1**	52.936 ± 4.815	33.515 ± 1.244	0.633
Complex **2**	63.182 ± 1.916	36.604 ± 1.056	0.579
Complex **3**	**35.172 ± 1.175**	37.941 ± 0.964	**1.078**
Complex **4**	43.751 ± 2.480	36.744 ± 0.159	0.838
Complex **5**	>100	80.267 ± 1.210	n/a
Complex **6**	>100	78.252 ± 1.501	n/a
Complex **7**	75.215 ± 4.733	46.913 ± 2.048	0.623
Complex **8**	>100	>100	n/a
Complex **9**	78.211 ± 8.658	69.301 ± 1.606	0.886
Cisplatin	2.78 ± 1.40	3.43 ± 0.48	1.233

complexes evaluated complex **3** was the most potent against both cell lines. The selectivity index (SI) is shown in Table 3, which is defined as the ratio of IC_{50} values in ARPE-19 cells divided by the IC_{50} of HCT-116 cells. Complex **3** was also the most selective of the novel complexes evaluated with equitoxic activity observed against both HCT-116 and ARPE-19 cells. Whilst these complexes were not as potent as cisplatin, complex **3** has a selectivity index that is comparable to cisplatin (SI = 1.078 and 1.233 respectively) and it is therefore the most promising complex in this series.

IC_{50} = concentration of the drug required to inhibit the growth of 50% of the cancer cells (μM)

4. Conclusion

In this work, we have successfully synthesized d^6 half-sandwich metal complexes bearing thiourea ligands and the reactivity of these complexes towards NaN_3. The ligands used in this work exhibited interesting binding modes on reacting with sodium azide. Further reactions of mono-dentate complexes **1**–**9** with NaN3 resulted in deprotonation of amido hydrogen and change the coordination mode of the thiourea derivative from mono-dentate to bidentate chelating mode. This complexes **10**–**18** coordinate in a highly strained four membered chelated $\kappa^2_{(N,S)}$ towards the metal atoms rather than the six membered chelated $\kappa^2_{(O,S)}$. As there are two amido groups in the thiourea derivative we expect the coordination of the other amido group as well, but the molecular structure revealed that only the amido adjacent to carbonyl group coordinates to metal which may be due to strong electron withdrawing property of aryl group. Chemosensitivity activity of the complexes carried out against HCT-116 cancer cell line displayed that some of the complexes are cytotoxic. Of these, complex **3** was the most potent and whilst its potency was less than cisplatin, its selectivity for cancer as opposed to non-cancer cell lines in vitro was comparable to cisplatin. Further we have carried out the antibacterial studies performed against four pathogenic bacteria viz., *S. aureus, E. coli*, *B. thuringiensis* and *P. aeruginosa* but none of the compounds showed any activity. The complexes were fully characterized by various spectroscopic studies and their molecular structures were established by single X-ray analysis.

Acknowledgements

Agreeda Lapasam thanks CSIR- HRDG Delhi, India for providing financial assistance in the form of JRF fellowship. We express our sincere thanks to Dr. Krishna Mohan Poluri, IIT Roorkee for their help to carry out the antibacterial studies. We thank DST-PURSE SCXRD, NEHU-SAIF, Shillong, India for providing Single crystal X-ray analysis and other spectral studies.

Appendix A. Supplementary data

Supplementary data to this article can be found online at https://doi.org/10.1016/j.jorganchem.2018.11.020.

CCDC **1874292** (**2**), **1874293** (**3**), **1874294** (**4**), **1874295** (**5**), **1874296** (**7**), **1874297** (**8**), **1874298** (**10**), **1874299** (**16**), contains the supplementary crystallographic data for this paper. These data can be obtained free of charge via www.ccdc.cam.ac.uk/data_request/cif, by e-mailing data_request@ccdc.cam.ac.uk, or by contacting The Cambridge Crystallographic Data Centre, 12, Union Road, Cambridge CB2 1EZ, UK; Fax: +44 1223 336033.

References

[1] B. Rosenberg, L. VanCamp, J.E. Trosko, V.H. Mansour, Nature 222 (1969) 385.
[2] F. Muggia, Gynecol. Oncol. 112 (2009) 275.
[3] B. Rosenberg, Adv. Exp. Med. Biol. 91 (1997) 129.
[4] R. Bieda, I. Ott, M. Dobroschke, A. Prokop, R. Gust, W.S. Sheldrick, J. Biol. Inorg. Chem. 103 (2009) 698.
[5] Z. Liu, P.J. Sadler, Acc. Chem. Res. 47 (2014) 1174.
[6] B.S. Murray, M.V. Babak, C.G. Hartinger, P.J. Dyson, Coord. Chem. Rev. 306 (2016) 86.
[7] J. Reedijk, Platinum Met. Rev. 52 (2008) 2.
[8] E.S. Antonarakis, A. Emadi, Cancer Chemother. Pharmacol. 66 (2010) 1.
[9] G. Süss-Fink, Dalton Trans. (2010) 1673.
[10] F.A. Khan, B. Therrien, G. Süss-Fink, O. Zava, P.J. Dyson, J. Organomet. Chem. 730 (2013) 49–56.
[11] (a) M. Haghdoost, J. Guard, G. Golbaghi, A. Castonguay, Inorg. Chem. 57 (2018) 7558;
(b) E. Alessio, Eur. J. Inorg. Chem. (2017) 1549.
[12] S. Thota, D.A. Rodrigues, D.C. Crans, E.J. Barreiro, J. Med. Chem. 61 (2018) 5805.
[13] S.J. Lucas, R.M. Lord, A.M. Basri, S.J. Allison, Roger M. Phillips, A.J. Blackera, P.C. McGowan, Dalton Trans. (2016) 6812.
[14] R.K. Gupta, R. Pandey, G. Sharma, R. Prasad, B. Koch, S. Srikrishna, P. Li, Q. Xu, D.S. Pandey, Inorg. Chem. 52 (2013) 3687.
[15] M. Melchart, A. Habtemariam, O. Novakova, S.A. Moggach, F.P.A. Fabbiani, S. Parsons, V. Brabec, P.J. Sadler, Inorg. Chem. 46 (2007) 8950.
[16] M.A. Scharwitz, I. Ott, Y. Geldmacher, R. Gust, W.S. Sheldrick, J. Organomet. Chem. 693 (2008) 2299.
[17] S.K. Singh, S. Joshi, A.R. Singh, J.K. Saxena, D.S. Pandey, Inorg. Chem. 46 (2007) 10869.
[18] S. Blanck, J. Maksimoska, J. Baumeister, K. Harms, R. Marmorstein, E. Meggers, Angew. Chem. Int. Ed. 51 (2012) 5244.
[19] S.P. Mulcahy, E. Meggers, Med. Organomet Chem, vol. 32, Springer, 2010, p. 141.
[20] S. Mollin, R. Riedel, K. Harms, E. Meggers, J. Inorg. Biochem. 148 (2015) 11.
[21] C. Kunick, I. Ott, Angew. Chem. Int. Ed. 49 (2010) 5226.
[22] N. Gunasekaran, P. Ramesh, M.N.G. Ponnuswamy, R. Karvembu, Dalton Trans. (2011) 12519.
[23] R.S. Correa, K.M. de Oliveira, F.G. Delolo, A. Alvarez, R. Mocelo, A.M. Plutin, M.R. Cominetti, E.E. Castellano, A.A. Batista, J. Inorg. Biochem. 150 (2015) 63.
[24] A. Mahajan, S. Yeh, M. Nell, C.E.J. van Rensburg, K. Chibale, Bioorg. Med. Chem. Lett 17 (2007) 5683.
[25] W.S.I. Lin, C.N. Lok, K. Yan, C.M. Che, Chem. Commun. 49 (2013) 3297.
[26] R.D. Campo, J.J. Criado, R. Gheorghe, F.J. Gonzalez, M.R. Hermosa, F. Sanz, J.L. Manzano, E. Monte, E.R. Fernandez, J. Inorg. Biochem. 98 (2004) 1307.
[27] Z.H. Li, Y. Zhang, Z.H. Peng, Y.G. Wang, Huaxueshiji 24 (2002) 214.
[28] N. Selvakumaran, N.S.P. Bhuvanesh, A. Endo, R. Karvembu, Polyhedron 75 (2014) 95.
[29] N. Selvakumaran, N.S.P. Bhuvanesh, R. Karvembu, Dalton Trans. (2014) 16395.
[30] K. Jeyalakshmi, J. Haribabu, N.S.P. Bhuvanesh, R. Karvembu, Dalton Trans. (2016) 12518.
[31] S. Saeed, N. Rashid, P.G. Jones, M. Ali, R. Hussain, Eur. J. Med. Chem. 45 (2010) 1323.
[32] M. Kalidasan, R. Nagarajaprakash, M.R. Kollipara, Trans. Met. Chem. 40 (2015) 531.
[33] M. Kalidasan, R. Nagarajaprakash, S. Forbes, Y. Mozharivskyj, M.R. Kollipara, Z. Anorg. Allg. Chem. 641 (2015) 715.
[34] (a) S. Adhikari, O. Hussain, R.M. Phillips, W. Kaminsky, M.R. Kollipara, Appl. Organomet. Chem. 32 (2018) e4362;
(b) S. Adhikari, O. Hussain, R.M. Phillips, W. Kaminsky, M.R. Kollipara, Appl. Organomet. Chem. 32 (2018) e4476.
[35] I.L. Mawnai, S. Adhikari, W. Kaminsky, M.R. Kollipara, J. Organomet. Chem. 869 (2018) 26.
[36] (a) M.A. Bennett, T.N. Huang, T.W. Matheson, A.K. Smith, S. Ittel, W. Nickerson, Inorg. Synth. 21 (1982) 74.
[37] (a) G.M. Sheldrick, Acta Crystallogr. Sect.A 46 (1990) 467;
(b) G.M. Sheldrick, Acta Crystallogr. Sect.A 64 (2008) 112.
[38] L.J. Farrugia, J. Appl. Crystallogr. 32 (1999) 837.
[39] (a) R. M Phillips, P.B. Hulbert, M.C. Bibby, N.R. Sleigh, J.A. Double, Br. J. Cancer. 65 (1992) 359;
(b) S. Adhikari, D. Sutradhar, S.L. Shepherd, R.M. Phillips, A.K. Chandra, M.R. Kollipara, Polyhedron 117 (2016) 404.
[40] K. Jeyalakshmi, J. Haribabu, C. Balachandran, N.S.P. Bhuvanesh, N. Emi, R. Karvembu, New J. Chem. 41 (2017) 2672.
[41] S. Adhikari, W. Kaminsky, M.R. Kollipara, J. Organomet. Chem. 848 (2017) 95.